Structural switching aptamer-based electrochemical sensor for mycotoxin patulin detection

Netice Küçük[a], Şevval Kaya[b], Samet Şahin[c,d], Mustafa Oguzhan Cağlayan[e,]*

[a] Bilecik Seyh Edebali University, Department of Biotechnology, Bilecik, Turkey
netice.kucuk@bilecik.edu.tr

[b] Bilecik Seyh Edebali University, Department of Biotechnology, Bilecik, Turkey
kayaasevval@gmail.com

[c] Bilecik Seyh Edebali University, Department of Bioengineering, Bilecik, Turkey
samet.sahin@bilecik.edu.tr

[d] School of Engineering, Lancaster University, Lancaster, LA1 4YW, UK s.sahin@lancaster.ac.uk

[e,*] Bilecik Seyh Edebali University, Department of Bioengineering, Bilecik, Turkey
oguzhan.caglayan@bilecik.edu.tr
e-mail: oguzhan.caglayan@bilecik.edu.tr (corresponding author)

Abstract

In this study, an electrochemical and aptamer-based aptasensor was developed for the sensitive detection of patulin, a mycotoxin commonly found in fruits and fruit-based products. The aptasensor used an innovative structural switching signal-off platform for detecting patulin. The aptamer immobilization on screen-printed carbon electrodes was achieved through Au electrodeposition and thiol group (-SH) route. Response surface methodology was used to determine the optimal incubation times for the aptamer, blocking agent, and target molecule, which were found to be 180 minutes, 40 minutes, and 89 minutes, respectively. The response of the aptamer to different concentrations of patulin was measured using square wave voltammetry by exploiting the structural switching mechanism. The sensor response was determined by quantifying differences in the aptasensor's background current. The aptasensor exhibited a linear working range of 1-25 µM and a low detection limit of 3.56 ng/mL for patulin. The aptasensor's relative standard deviation and accuracy were determined to be 0.067 and 94.4%, respectively. A non-specific interaction was observed at low concentrations of two other mycotoxins, ochratoxin A and zearalenone. The interference from ochratoxin A in the measurements was below 10%. In real sample tests using apple juice, interference, particularly at low concentrations, had changed the recovery of patulin negatively with a significant effect on the structural switching behaviour. Nevertheless, at a concentration of 25 ng/mL, the interference effect was eliminated, and the recovery standard deviation improved to 6.6%. The aptasensor's stability was evaluated over 10 days, and it demonstrated good performance, retaining 13.12% of its initial response. These findings demonstrate the potential of the developed

electrochemical aptasensor for the sensitive detection of patulin in fruit-based products, with prospects for application in food safety and quality control.

Keywords: Patulin, aptasensor, square wave voltammetry, structural switching, apple-juice

1. Introduction

Food safety is a critical subject that necessitates the implementation of consistent precautions and robust monitoring throughout the entire food supply chain, from agricultural production to consumption. This comprehensive process encompasses various stages, including the sourcing of raw materials, food processing, the attainment of the final product, and its subsequent storage [1]. To enhance the effectiveness of analytical techniques employed for identifying hazardous constituents in food samples, it is of utmost importance to advance the development of novel receptors that exhibit heightened affinity towards specific targets. These receptors play a pivotal role in enabling the rapid, sensitive, and reliable detection of potentially harmful components [2].

Mycotoxins are secondary metabolites with a relatively low molecular weight (around 700 Da) that have the potential to contaminate a wide range of agricultural commodities. This contamination can occur at different stages, including during cultivation in the field and storage [3]. These toxic compounds can enter the human food chain either through direct consumption or indirectly through the consumption of animal-derived products from animals that have ingested feed contaminated with mycotoxins [4]. More than 100 fungal species have been identified as producers of approximately 400 potentially toxic mycotoxins [5, 6]. These mycotoxins, including trichothecenes, ochratoxins, aflatoxins, zearalenone, fumonisins, patulin, and citrinin, are considered highly toxic and pose significant risks to agriculture, livestock, and public health [7].

Patulin (PAT) is a specific mycotoxin known to contribute to the toxicity of food, with a notable presence in apples [8-11]. It is classified as a secondary metabolite produced by various fungal species, such as *Penicillium expansum* (*P. leucopus*), *P. patulum* (*P. urticae, P. griseofulvum*), *P. crustosum*, and *A. clavatus* [12, 13]. PAT, characterized by its low molecular weight, water solubility, and thermal stability [14], represents a significant global food safety concern. It is frequently encountered in fruits and vegetables owing to their high moisture and sugar content. The severity of acute PAT poisoning's detrimental effects on various organs [15] escalates in correlation with the ingested quantity [16]. Consequently, the consumption level of contaminated food assumes crucial importance, particularly among infants and children [17]. To mitigate the risks associated with acute and chronic PAT exposure, regulatory bodies such as the World Health Organization (WHO), the Food and Agriculture Organization (FAO), and the European Commission (EC) have established guidelines,

setting a maximum tolerable daily intake of 0.4 μg/kg body weight/day, restricting the maximum PAT concentration in fruit juices to 50 μg/kg, and imposing a limit of 10 μg/kg for baby food products [16, 18]

Conventional methods employed for PAT detection, such as high-performance liquid chromatography (HPLC) and enzyme-linked immunosorbent assays (ELISAs [19]), offer high reliability [20-22]. However, they suffer from limitations including time-consuming sample preparation, the need for skilled personnel, and the requirement for expensive equipment. These constraints hinder their practical application in field settings [23, 24] Given the acute symptoms observed in both humans and animals [25], as well as the genotoxic, mutagenic [26], immunotoxic, neurotoxic [27], and teratogenic [28] properties associated with PAT, rapid and facile detection methods are of paramount importance for ensuring human health and food safety. To overcome these challenges and enable rapid on-site analysis, the development of innovative sensing platforms becomes imperative. Promising avenues in this regard include aptamer-based, enzyme-based, and antibody-based biosensors [9, 13, 18]. Aptamers are single-stranded oligonucleotides composed of DNA or RNA that are derived from a random or combinatorial library [29, 30]. These aptamers possess the ability to specifically interact with target molecules, resembling the interactions observed between antibodies and antigens [31]. The process of aptamer generation involves a technique called systematic evolution of ligands by exponential enrichment (SELEX), which entails iterative rounds of exponential enrichment to select aptamers with high affinity for a specific target [32]. The simplicity and effectiveness of aptamer generation via SELEX have positioned them as promising alternatives to antibodies, overcoming their fragility and challenging production, leading to their designation as "synthetic antibodies" [33-35]. Notably, DNA-based aptamers exhibit enhanced stability compared to antibodies. Their remarkable stability, exceptional selectivity, and facile surface modification capabilities render aptamers optimal molecular recognition elements for various biosensor applications [36]. Moreover, aptamers offer several advantages such as the detection of small molecules, facile detachment from immobilized surfaces, reusability, and cost-effectiveness [37]. Despite the significant prevalence of PAT as a contaminant and its consequential economic and public health risks, there is a noteworthy scarcity of research studies employing aptamer-based approaches for the specific detection of this mycotoxin [16].

In recent years, aptamer-based sensors have emerged as highly promising tools for the detection of diverse analytes. Various transduction techniques, including electrochemical, optical, and spectroscopic methods, have been employed in aptasensors for mycotoxin detection. Khan *et al.* reported the development of a fluorescence-based aptasensor for the detection of PAT in apple wine samples, yielding toxin recoveries ranging from 96% to 98% [23]. Ma *et al.* described a fluorometric PAT sensor based on a combination of magnetic nanoparticles, reduced graphene oxide (rGO), and DNase I, achieving a remarkable detection limit of 0.28 ng/mL [38]. A study focusing on a homogeneous fluorescent aptasensor, with broad applicability for the detection of various food contaminants, demonstrated excellent performance of the PAT aptasensor in apple juice within a linear

dynamic range of 0.05-1 ng/mL [39]. For the detection of PAT in apple juice, a sophisticated fluorescent aptasensor was developed using sulfur quantum dots encapsulated in MOF-5-NH_2 and a self-cycling catalytic hairpin assembly (scCHA) system. The results obtained exhibited a strong correlation with HPLC analysis, confirming the aptasensor's exceptional specificity, anti-interference capability, and reproducibility [40]. Gua *et al.* devised a surface-enhanced Raman scattering (SERS) aptasensor by integrating a signal molecule and chitosan-modified magnetic nanoparticles with a gold-silver core-shell structure. This aptasensor achieved remarkable recovery rates ranging from 96.3% to 108% in real apple juice samples [41].

The simplicity of operation, fast response time, and potential for portability are advantageous features of electrochemical sensors [42]. Moreover, the strong affinity of aptamers for their target ligands has gained significant attention in the field of biosensor development[43]. Exploiting the benefits of both electrochemical sensors and aptamers, electrochemical platforms have been developed for the rapid detection of PAT [44]. To improve the sensitivity of these electrochemical biosensors, various nanomaterials have been employed to enhance signal amplification [45].

In a study conducted by Liu *et al.*, a panel of four distinct aptamers harboring diverse PAT sequences was employed in electrochemical (EC) and photoelectrochemical (PEC) experiments to elucidate their detection behaviors on electrode surfaces [42]. Through meticulous evaluation, the most optimal aptamer was identified, demonstrating remarkable sensitivity in the detection of PAT within apple puree samples, with detection limits of 30 fg/mL and 50 fg/mL [46]. In a subsequent investigation by Xu *et al.* in 2019, an impedimetric methodology was adopted to develop a PAT sensor, wherein graphene-like black phosphorus nanosheets (BP NSs) were strategically employed for the surface modification of a glassy carbon electrode (GCE) [45]. Further enhancements were achieved by functionalizing the BP-NS-GCE interface with gold nanoparticles and thiolated PAT aptamer, resulting in a significantly reduced detection limit [47]. Another study implemented a dual-signal strategy for PAT detection, leading to the development of a highly sensitive aptasensor. Notably, the synthesis of a gold nanoparticle-black phosphorus heterostructure (AuNPs-BPNS) was executed to effectively amplify the sensing performance. This aptasensor demonstrated a wide dynamic range spanning from 0.1 nM to 100.0 μM, along with an impressively low detection limit of 0.043 nM [12].

The response mechanism of an electrochemical sensor through structural aptamer switching involves the direct transfer or tunnelling of the redox moiety signal, facilitated by a conformational change induced upon the interaction of an aptamer modified with a redox center, such as methylene blue (MB), with a small-molecule target like PAT [48]. This process is depicted in Figure 1, where an initial signal is received (on) but subsequently diminishes (off) following the interaction. Structural switching aptamer-based electrochemical sensors have been documented to demonstrate low detection limits across diverse applications [49].

Incubation time and analyte concentration are among the parameters that have a profound effect on biosensor performance [50]. Response surface methodology (RSM) is widely used for optimization of

foodborne pathogen detection in label-free electrochemical nucleic acid biosensors. RSM is a combination of statistical and mathematical techniques used to design experiments, build models, evaluate the influence of factors, and seek optimal conditions for desired responses. The traditional practice of changing one variable at a time does not allow for evaluation of the combined effects of all factors involved in the process. This creates a time-consuming methodology. [51]. It may lead to misleading results due to overlapping interactions between input parameters. It should be noted that sometimes these interactions may be more important than the effect of the independent variables. [52] These limitations can be overcome by the use of RSM, which can identify and quantify various interactions between different parameters.[51] In this study, it was aimed to obtain maximum efficiency and minimum cost by using the RSM method.

This manuscript presents an electrochemical sensor based on aptamer switching for the selective and sensitive detection of PAT. The sensor utilizes the principle of target-induced aptamer switching, where the presence of PAT induces a conformational change in the aptamer, resulting in an observable electrochemical signal. The developed sensor offers notable advantages, including simplicity, rapid response time, affordability, and portability, rendering it a promising candidate for on-site PAT detection in diverse food matrices. Additionally, the design, fabrication, and characterization of the aptamer-based sensor are thoroughly elucidated, along with its performance in detecting PAT in commercially available apple juice. Comparative analysis with conventional methods highlights the sensor's analytical capabilities and underscores its potential as an alternative approach for PAT detection.

2. Materials and Methods

2.1. Instruments and Chemicals

All electrochemical measurements in this study were conducted using an Ivium potentiostat (Ivium Technologies, B.V., Netherlands) at a controlled temperature of 23±2°C. Screen-printed electrodes (SPEs, DRP-110) with a working electrode area of 0.126 cm^2 were purchased from a local distributor of Dropsens. Chemicals employed in the experiments were procured from Sigma-Aldrich, unless otherwise specified, and were of analytical grade. UPW with a resistivity of 18.2 MΩ·cm was used for the preparation of aqueous solutions and rinsing steps. The MB-modified PAT aptamer probe (MB-aptamer), specifically designed for the recognition of PAT selected from the literature [50] was obtained from Ella Biotech (Germany). The nucleotide sequence and seconder structure at 23°C of the MB-aptamer is given in Table S1 [50, 51]. The lyophilized aptamer was utilized without any additional treatment and used as is.

2.2. Instruments and Chemicals

2.2.1. Au electrodeposition

SPEs were initially subjected to electrochemical cleaning using the linear sweep voltammetry (LSV) technique. This involved applying a potential step of 1 mV in the range of 0 to -2 V with a scan rate of 20 mV/s in 0.1 M KCl. The purpose of this step was to eliminate impurities and ensure a clean surface for the electrodes. After the electrochemical cleaning process, the SPEs were dried, and a solution containing 1 mM chloroauric acid $[AuCl_4]^-$ in 0.1 M KCl was drop-cast onto the surface of the electrodes. This step aimed to facilitate the deposition of a thin layer of gold (Au) on the electrode surface. Subsequently, the coated electrodes, referred to as SPE/Au, were subjected to cyclic voltammetry (CV) with 15 cycles in the range of 0 to -1.5 V at a scan rate of 50 mV/s [33]. This electrochemical process induced the deposition of a visible layer of Au on the electrode surface, thereby enhancing its sensitivity and performance. After the electrodeposition process, the SPE/Au electrodes were washed with ultrapure water (UPW) to remove any residual impurities. They were then dried ensuring they were free from moisture and ready for the subsequent step of aptamer immobilization.

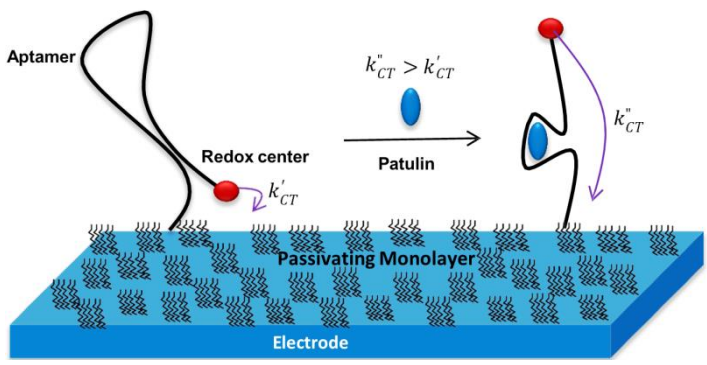

Fig. 1. The schematic representation of the principle of structural switching aptasensor platform for PAT detection.

2.2.2. Aptamer immobilization

Aptamer immobilization was carried out using MB-modified aptamers with the sequence SH-$(CH_2)_6$-Aptamer-AttoMB2. A 10 µM solution of MB-aptamer in pH 7.4 phosphate-buffered saline (PBS) containing 0.1 M PBS with 0.05% Tween-20 was prepared. A volume of 10 µL of the 10 µM MB-aptamer solution (0.05% Tween-20 PBS) was applied to the surface of the SPE-Au electrode and allowed to interact with the Au surface. Following incubation, the electrode was rinsed with the same buffer and subsequently treated with 1 mM 6-mercapto-1-hexanol (MCH) to block the Au surface. Surface active molecules were generally used to both reduce non-specific interactions [55] and

improve immobilization by balancing the interaction of the aptamer with the Au surface during the immobilization stage of the aptamer [56]. The addition of Tween-20 in the buffer was intended to enhance the interaction between the aptamer and the target analyte [52]. Finally, the electrodes were washed with buffer and prepared for the detection of the target analyte (PAT) as SPE-Au/Apt.

To determine the presence of PAT, the electrodes incubated with different concentrations of PAT in the buffer were subjected to square wave voltammetry (SWV). The SWV measurements were performed within the potential range of (-0.8) to (-0.3) V, using a single scan, a signal magnitude of 10 mV, and a frequency of 25 Hz. The same procedure was repeated after incubating the electrodes with PAT, and the resulting change in current between the two scenarios was recorded as the response of the aptasensor. The overall schematic representation of the modification steps of the SPE/Au/Apt electrode for the detection of PAT is given in Figure 2.

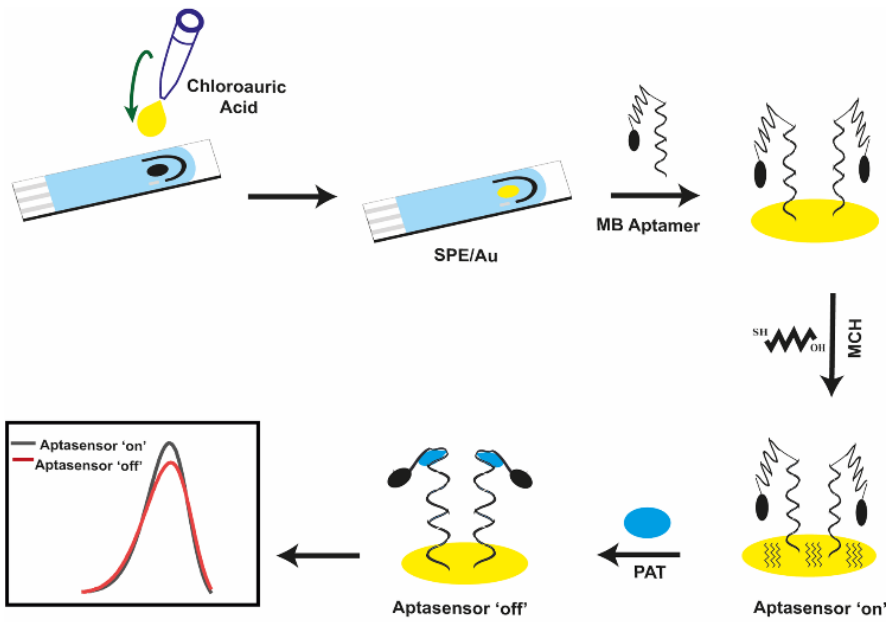

Fig. 2. The schematic representation of the production steps of the structural switching electrochemical aptasensor for PAT detection [33].

2.2.3. Determination of the optimal aptamer, MCH, and PAT incubation duration times

To determine the optimal incubation times for aptamer, MCH, and PAT, the response surface method (RSM), a central composite design method, was utilized in the optimization studies. RSM analysis, based on the response of the PAT aptasensor, was performed to examine the relationship between the aptamer, MCH, and PAT incubation times and the resulting current change. Statistical evaluations were conducted, and the analysis results indicated that the quadratic method provided the most suitable model for the experimental data. The experimental plan for the optimization studies, which focused on aptamer modification, MCH modification, and PAT incubation time as key factors, along

with the determined optimum values based on statistical evaluations and the desirability function, can be found in Table S2, Figure S1 [33].

2.3. Determination of Analytical Performance

The analytical performance of the SPE-Au/Apt electrodes was assessed using the SWV technique with the electrodes initially tested in a PAT-free 0.1 M PBS (pH 7.4) solution to establish the baseline response. Subsequently, the electrodes were incubated with various concentrations of PAT (1, 2, 5, 10, 25 ng/mL in 0.1 M PBS, pH 7.4) for 89 minutes. Following the incubation, the electrodes were thoroughly washed with 0.1 M PBS (pH 7.4). The prepared SPE-Au/Apt/PAT electrodes were tested using SWV in 0.1 M PBS (pH 7.4) solution, and the resulting current change between the two conditions was recorded as the response of the aptasensor.

The calibration curve was constructed by plotting the maximum current change against the corresponding PAT concentration. The calibration experiments were repeated three times using different electrodes, and the standard deviation of the data points was determined. After calibrating the aptasensor, the limit of detection (LOD) was calculated as 3 times the standard deviation (3σ) within a 95% confidence interval, where σ represents the largest standard deviation observed among the repeated measurements.

2.4. Interference, Real Sample, and Stability Tests

Interference experiments were performed to assess the potential interference of two common mycotoxins, OTA A (OTA-A) and ZEN, on the detection of PAT. During the optimized incubation period, the current values resulting from the incubation of these interferents were examined. The SPE-Au/Apt electrodes were initially tested without PAT, followed by incubation with concentrations of 5 ng/mL and 25 ng/mL of ZEN (PAT+ZEN) and OTA-A (PAT+ZEN+OTA), respectively. The experiments were repeated three times (N=3) to ensure reliability and reproducibility.

For real sample testing, apple juice samples obtained from local markets were processed by mixing them with an equal volume of ethyl acetate solution (99.5% purity, obtained from Merck) using a vortex mixer, followed by centrifugation. The upper ethyl acetate phase (1 mL) was collected after phase separation and diluted with 19 mL of PBS. Different concentrations of PAT (5 ng/mL, 10 ng/mL, and 25 ng/mL) were added to these prepared apple juice samples using the standard addition method. The measured values were then compared with the calibration curve to assess the accuracy of PAT detection in real samples.

Stability experiments were conducted to evaluate the electrode stability. The prepared SPE-Au/Apt electrodes were stored at +4°C for 10 days after obtaining the baseline current value. After the storage period, the electrodes were tested with PAT, and the percentage change in the current difference value

was calculated relative to the reference value. Furthermore, the electrodes were stored at +4°C for an additional 10 days and tested again to assess the sensor response compared to the reference value.

3. Results and Discussion

3.1. Au electrodeposition and aptamer immobilization

The CV results depicting the Au electrodeposition on the SPEs are illustrated in Figure 3 (a). It was observed that the Au coating reached a steady state with no significant changes in the voltammogram after the initial three cycles. Subsequently, after 15 cycles, the surface was entirely coated resulting in a visibly discernible layer of Au.

To optimize the performance of the electrode, the modification of the aptamer and MCH, as well as the incubation durations for the target molecule (PAT), were conducted using RSM. The detailed RSM experimental design can be found in Table S3, S4. The relationship between the durations of aptamer, MCH, and PAT incubation and the resulting change in current were investigated based on the response of the electrochemical PAT sensor. A higher current difference was preferred compared to the bare electrode. Statistical evaluations indicated that the quadratic method provided the most suitable model for the experimental data. Using the solution where the desirability function equalled 1, the optimized values for the aptamer, blocking agent (MCH), and target molecule incubation durations were determined as 180 minutes, 40 minutes, and 89 minutes, respectively. These optimized values were subsequently employed for the production and analysis of Au-coated SPE electrodes in the subsequent stages of the study.

The on-off sensor response, based on the molecular switching phenomenon, was evaluated in the presence of PAT, and the results are presented in Figure 3 (b) for a PAT concentration of 25 ng/mL. The electron transfer between the electrode and the MB probe allows for a current response, resulting in the aptasensor being in the "on" state when PAT is absent. Conversely, incubation with PAT blocks the current, leading to the aptasensor being in the "off" state. This "on-off" behavior suggests that the electron transfer distance may depend on the number of PAT molecules bound to the aptamer, enabling calibration for the quantitative measurement of PAT concentration in a given sample.

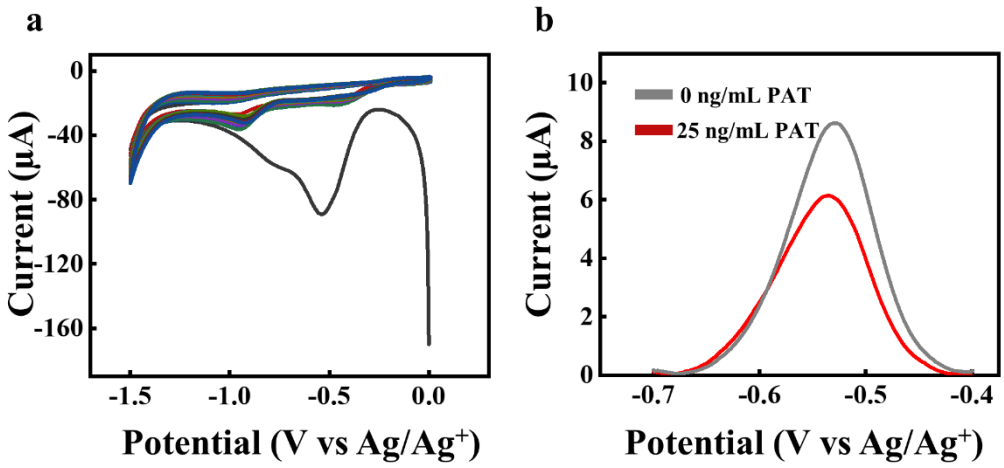

Fig. 3. (a) CVs for 1 mM [$AuCl_4$]-electrolysis at 0.1 M KCl at 50 mV for 15 cycles (b) Signal on-off signal response of the Aptasensor to PAT.

3.2. Determination of the Analytical Performance

The peak current density values obtained from electrodes incubated with PAT solutions of different concentrations (1, 2, 5, 10, 25 ng/mL in 0.1 M PBS, pH 7.4) were plotted to examine the changes in response. The calibration curve of the developed aptasensor is presented in Figure 4. The calibration curve was generated by conducting three replicates at each of the five PAT concentrations and calculating the average values. It was observed that the structural switching mechanism resulted in a proportional decrease in current intensity as the PAT concentration increased. This proportionality became more pronounced starting from a PAT concentration of 2 ng/mL, exhibiting a higher level of linearity (determination coefficient R^2 = 0.993). At lower PAT concentrations, it is expected that the switching events may not occur in sufficient numbers to produce a significant change in current intensity. However, within the range of 2 ng/mL to 25 ng/mL, the switching behavior displayed a highly linear relationship with a high coefficient of determination. Additionally, the repeatability analysis showed an average standard deviation of 0.055 μA and a maximum deviation of 0.067 μA. This deviation corresponds to 5% of the measured sensor signal for 1 ng/mL PAT, indicating that the repeatability results demonstrate satisfactory analytical performance [53, 54].

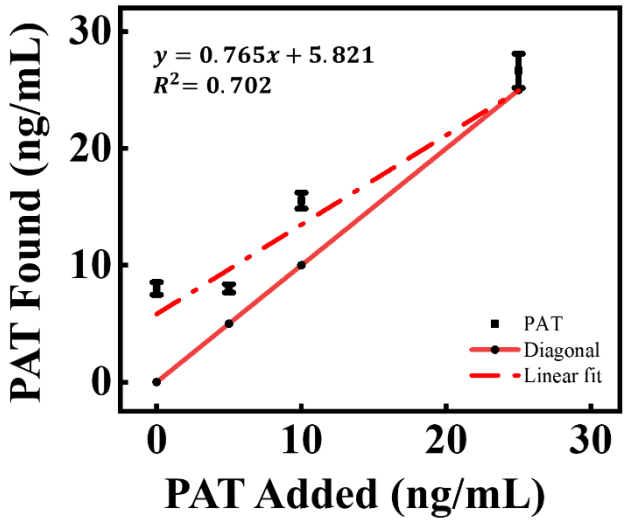

Fig. 4. Calibration curve for PAT detection of the aptasensor

The analytical parameters derived from the calibration curve are provided in Table 1. By fitting the data to the linear equation y=0.06238[PAT]+0.94567, which exhibits a determination coefficient R^2 of 0.94, LOD was determined using the relationship (3.3xσ)/slope. Here, the maximum σ value of 0.067 µA, obtained from the measurements, was utilized. The LOD was calculated to be 3.56 ng/mL [33]. Alternatively, if the calibration curve is initiated from 2 ng/mL, the equation y=0.05654[PAT]+1.04377 would provide an excellent fit to the data with an R^2 value of 0.99. In this case, the calculated LOD would be 3.91 ng/mL. Notably, both LOD values are quite close to each other, indicating a negligible absolute proportional difference of approximately 9% between the sensor sensitivity (slope of the calibration curve).

Table 1. The analytical parameters for the aptasensor

Analytical parameters	Values
Linear range (ng/mL)	1 to 25
Curve equation, i (µA), [PAT] (ng/mL)	i=0.0624[PAT]+0.9457
Sensitivity (ng PAT/µA.mL)	0.0624
Std. error of the slope, ±	0.0076
Std. error of the intercept, ±	0.946
R2	0.944
LOD ng/mL	3.56
LOQ ng/mL	10.7

Balance analysis of the model, comparison of model estimation results with actual results, change of current values for Aptamer modification time, MCH modification time and PAT incubation time, the

relationship of aptamer and MCH modification time with current according to RSM results, the current relationship of aptamer modification PAT incubation time according to RSM results, MCH modification time and current relationship of PAT incubation time according to RSM results.

3.3. Interference, Real Sample, and Stability Tests

The influence of interfering substances, OTA and ZEN, on the response of the aptasensor was investigated at concentrations of 5 ng/mL and 25 ng/mL for each substance. This analysis was conducted using four electrodes, and the corresponding values, obtained from the calibration curve, along with the standard deviation, are depicted in Figure 5.

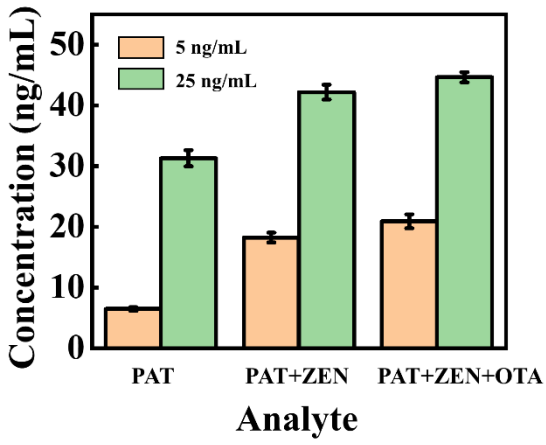

Fig. 5. The impact of interfering substances on the response of the aptasensor. Response at a concentration of 5 ng/mL and 25 ng/mL of the interfering substance. The error bars represent the standard deviations of the samples, derived from four independently prepared electrodes.

The aptamer used in this study, which specifically binds to PAT, has been previously reported in the literature [50]. On the other hand, it was observed that when potential interferents including ZEN and OTA were co-incubated with 5 ng/mL of PAT on the sensor surface, the measured values obtained from the calibration curve exhibited a positive bias. In particular, ZEN caused a significant increase in the sensor response at a concentration of 5 ng/mL, resulting in a response equivalent to concentrations above 15 ng/mL. However, this non-specific interference effect was not observed at a higher ZEN concentration (25 ng/mL). It is evident that, apart from the competitive interaction of ZEN with the PAT-specific aptamer at low concentrations, ZEN also induces a structural interaction that enhances the rate of signal decrease. The physicochemical properties of PAT, ZEN, and OTA were calculated using molecular mechanics (MM2) modeling, and the results are summarized in the Table S5. The calculated parameters, including LogP, total connectivity, and topological index (Wiener), differ as expected for PAT, ZEN, and OTA. Although OTA is structurally closer to PAT compared to ZEN, it exhibited a lower non-specific interaction with the aptamer compared to ZEN. OTA alone generated an interfering signal of approximately 10% of the measured PAT concentration. When both interferents

interacted simultaneously, a similar positive bias of around 10% was observed. On the other hand, ZEN, which is more hydrophobic compared to the others, exhibited a non-specific interaction that could lead to a decrease in current through structural switching or interaction with the redox center. Interestingly, this negative interaction decreased at higher ZEN concentrations. However, in this study where the PAT-specific aptamer was selected and validated for different interferents, it cannot be definitively concluded that the aptamer interacts non-specifically with ZEN. Instead, it can be inferred that there is an interference in the aptamer switching or the interaction of the redox center with the electrode surface. Nevertheless, in practical applications, since ZEN is not a contaminant in apple juice [55], the mentioned interference may not significantly affect the analytical performance of the sensor.

In the real sample experiments, apple juice samples obtained from a local market were spiked with specific concentrations of PAT using the standard addition method. The recovery percentages and real sample data, expressed as the relative standard deviation (%RSD), are presented in Figure 6. The results demonstrated a positive bias, with higher values obtained at lower concentrations of the added PAT. Despite the linearity of the developed sensor's response to PAT, it was observed that there was no inherent PAT contamination in the real samples. However, competitive interference occurred, particularly at lower concentrations. Nevertheless, the high precision exhibited by repeat measurements, as indicated by the low %RSD, suggested that the proposed sensor platform could be directly employed for PAT detection in actual apple juice samples.

Moreover, the response of the sensor to the added PAT exhibited linearity, as evidenced by a R^2 of 0.80, albeit with a slope less than 1. This observation implies that at higher concentrations, such as the recommended 25 ng/mL for the sensor platform, the discrepancy between the added PAT concentration and the measured PAT response would diminish. It is important to note that the apple juice samples were directly applied onto the aptasensor without any pre-treatment to extract possible PAT contaminants. Despite this, the obtained standard error at the 25 ng/mL level was 6.6%, which represents an acceptable level of analytical performance. Consequently, it is anticipated that the suggested sensor platform can be effectively utilized for detecting PAT residues in apple juice, even at the maximum allowed residue level of 50 ng/mL.

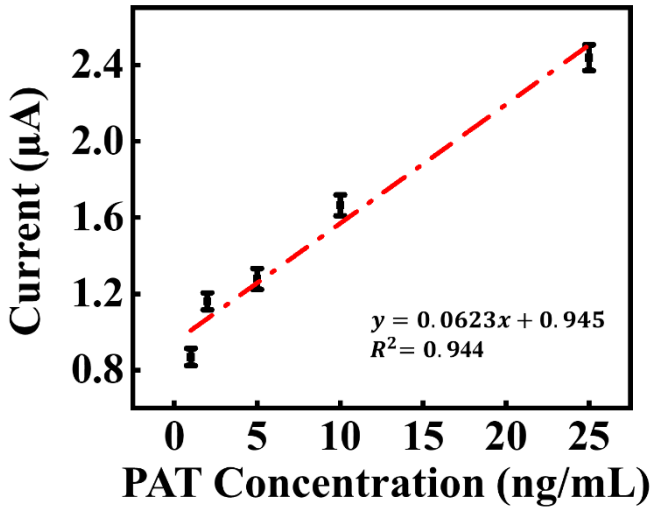

Fig. 6**.** Detected levels of PAT in apple juice using the standard addition method (two sample, N=3).

In the final phase of the study, the stability of the fabricated aptasensors was evaluated. The stability assessment relied on calculating the percentage change in the aptasensor response after a 10-day storage period at refrigeration conditions. Following the 10-day storage period, the aptasensor response exhibited a 13.12% (N = 3) positive bias relative to the initial response obtained for 5 ng/mL PAT. This observation suggests that the aptasensor maintained its performance for 10 days.

4. Conclusion

In this study, our objective was to develop a modified aptamer-based sensor for the highly selective and sensitive detection of PAT using the aptamer reported by Wu et al. [50]. The aptamer was suitably modified to enable its immobilization onto an Au-coated electrode surface, thereby facilitating the structural switching with the on-off signal capability of the sensor. MB was utilized as a modifier to facilitate the immobilization of the modified aptamer on the gold surface, ultimately leading to the development of the aptasensor.

To optimize the performance of the aptasensor, incubation durations of the aptamer, as well as the duration of the MCH and PAT incubation, were systematically investigated using the RSM method. The aim was to minimize errors and test duration. As a result, the optimal modification durations were determined as 180 minutes for the aptamer, 40 minutes for the MCH modification, and 89 minutes for the PAT incubation. The aptamer utilized in this study demonstrated the electrochemical on-off behavior of the aptasensor, where the presence of PAT induced a signal change.

The selected aptasensor exhibited a linear working range of 1-25 ng/mL, and the LOD was calculated to be 3.56 ng/mL with a 95% confidence interval determined by 3 times the standard deviation (3σ). To assess the performance of our developed aptasensor, we compared these range and LOD values with those reported in the literature for other electrochemical detection methods

(Table S6). The results indicated that our aptasensor holds significant potential for the accurate detection of PAT.

In this study, we have successfully developed an electrochemical sensor based on aptamer switching for the selective and sensitive detection of PAT, a mycotoxin that poses a significant concern in terms of food safety. Our sensor presents several advantages compared to conventional electrochemical methods for PAT detection, including a simplified assay procedure, enhanced specificity, and improved sensitivity. While the developed aptasensor has demonstrated promising results for the convenient and sensitive detection of PAT in buffer solutions, it is advisable to apply sample pre-processing steps or utilize the aptasensor for higher concentrations (> 25 ng/mL) of PAT detection in real samples. The latter recommendation is particularly relevant when analyzing apple juice, where the maximum residue limit set by the authorities is 50 ng/mL.

In conclusion, the aptamer switching electrochemical sensor presented in this manuscript represents a promising solution for PAT detection. The sensor's high sensitivity, selectivity, simplicity, and potential for on-site analysis make it an attractive candidate for the mycotoxin analysis.

Acknowledgements

This study was financially supported by the Scientific and Technological Research Council of Turkey (TÜBİTAK) under Project No. 121Z592. The authors would like to express their gratitude to TÜBİTAK for the financial support provided. They also extend their appreciation to Bilecik Şeyh Edebali University for the infrastructure support.

Data Availability Statement

Research data are not shared

Supplementary Material

Table S1**.** Sequences and secondary structure of MB-aptamer [50, 51]

Sequence	Secondary structure
5'- SH- $(CH_2)_6$- GGCCC GCCAA CCCGC ATCAT CTACA CTGAT ATTTT ACCTT-AttoMB2-3'	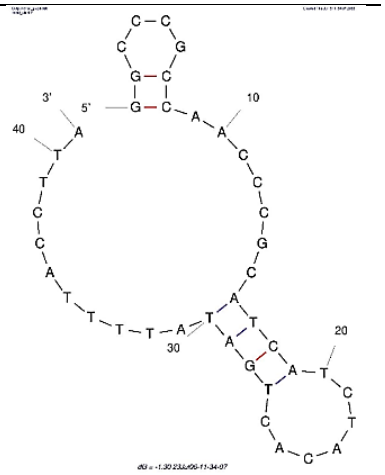

The experiments performed to determine the effect of aptamer and MCH modification and PAT incubation times on electrode performance were determined with the Design Expert program, and the experimental plan is given in Table S2.

Table S2**.** RSM experimental plan according to immobilization parameters.

Std	Exp.	Factor 1 A: Aptamer Modification	Factor 2 B: MCH Modification	Factor 3 C: PAT Incubation
4	1	150	60	90
18	2	150	60	47,5
17	3	150	60	47,5
10	4	240	60	47,5
9	5	60	60	47,5
7	6	60	90	90
5	7	60	30	90
6	8	240	30	90
2	9	240	30	5
13	10	150	60	5
20	11	150	60	47,5
3	12	60	90	5
15	13	150	60	47,5
12	14	150	90	47,5

19	15	150	60	47,5
16	16	150	60	47,5
8	17	240	90	90
11	18	150	30	47,5
1	19	60	30	5
4	20	240	90	5

To determine the effect of aptamer and MCH modification and PAT incubation times on electrode performance, experiments were carried out and analyzed with the Design Expert program, and the results are given in Table S3.

Table S3**.** Experiments determined by the Design Expert program and the results obtained

	Factor 1	Factor 2	Factor 3	Results
Exp.	A:Aptamer Modification Time (minute)	B:MCH Modification Time (minute)	C:PAT Incubation Time (minute)	Current (µA)
1	150	60	47,5	1,566
2	60	90	5	1,201
3	150	60	47,5	1,934
4	150	60	47,5	1,57
5	150	60	47,5	2,037
6	60	30	5	1,335
7	240	90	5	1,701

In the RSM analysis performed based on the PAT aptasensor response, the relationship of aptamer, MCH and PAT incubation times with the change in current was examined. According to the analysis results obtained as a result of the statistical evaluations, the quadratic method, which gave the best results, was recommended as the most suitable model for the experimental data. Statistical evaluations of the results obtained are given in Table S4 and their graphs are given in Figure S1.

Table S4**.** ANOVA results of the data in Table 3

Source	Sum of Squares	Degrees of Freedom	Mean Squares	f-Value	p-Value

Model	0,3616	3	0,1205	2,01	0,2900	not significant
A-Aptamer Modification Time	0,1250	1	0,1250	2,09	0,2442	
B-MCH Modification Time	0,0090	1	0,0090	0,1500	0,7244	
C-PAT Incubation Time	0,0893	1	0,0893	1,49	0,3093	
AB	0,0000	0				
AC	0,0000	0				
BC	0,0000	0				
AÂ²	0,0000	0				
BÂ²	0,0000	0				
CÂ²	0,0000	0				
Pure Error	0,1796	3	0,0599			
Cor Total	0,5412	6				

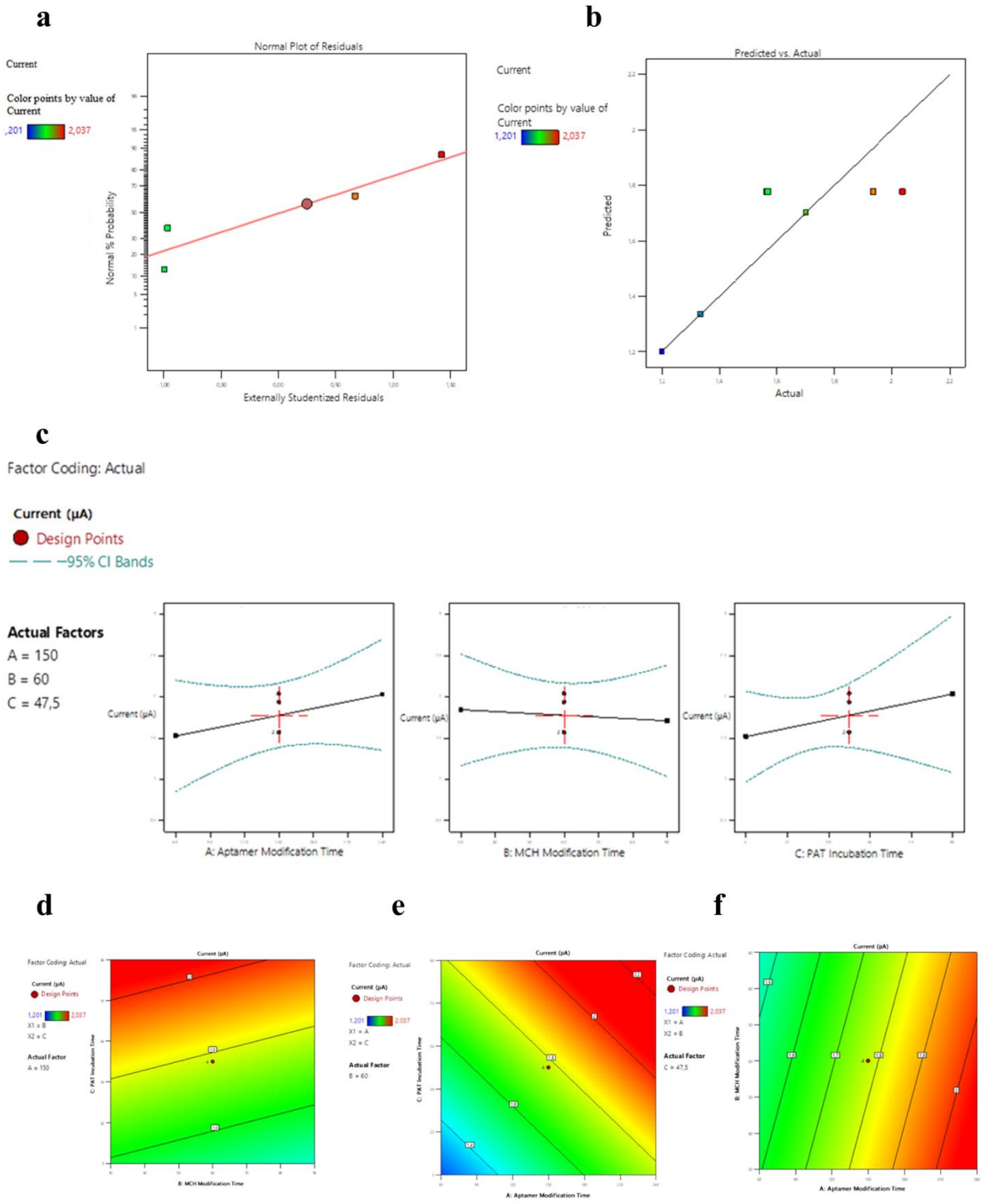

Fig. S1. (A) Residual analysis of the model, (B) comparison of model prediction results and actual results, (C) Change of current values for Aptamer Modification Time, MCH Modification Time and PAT incubation Time, (D) Relationship of Aptamer and MCH modification time with current according to RSM results, (E) Relationship between Aptamer modification and PAT incubation time and flow according to RSM results, (F) Relationship between MCH modification time and PAT incubation times with current according to RSM results.

Table S5 – Physicochemical properties, 1-4 van der Waals factor and Wiener index calculated for entrepreneurs ZEN and OTA with PAT.

	PAT	ZEN	OTA
Molecular structure	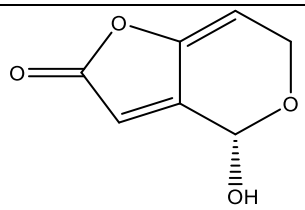	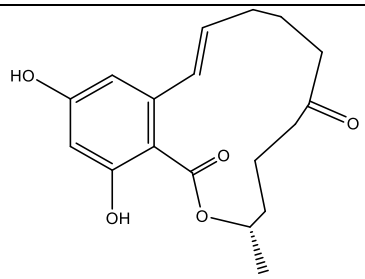	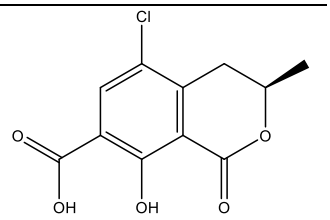
Stretch	0.3975	3.3788	2.7855
Bend	14.2503	14.2710	8.9576
Stretch-Bend	0.0877	0.6306	0.0567
Torsion	1.1177	15.1357	-0.7561
Non-1,4 VDW	-2.0779	-1.9683	-4.0717
1,4 VDW	4.1251	18.1306	14.5069
Dipole/Dipole	0.9734	3.1423	4.4234
Total Energy	18.87 kcal/mol	52.72 kcal/mol	25.90 kcal/mol
LogP	-0.928	3.316	1.877
Total Connectivity	0.019642	0.000473	0.004365
Wiener Index	139	1150	460

Table S6 **-** Comparison of some aptamer-based PAT sensors and chromatographic methods reported in the literature.

Method	Approach	LOD(ng/mL)	Range(ng/mL)	Ref.
Fluorescence	Carboxy-fluorescein dye and –COOH functionalized MWCNT quencher	0.13	5-350	[56]
Fluorescence	FRET, fluorescent tagged oligomer release activated with DNA duplex removal and analyte interaction	$6x\ 10^{-3}$	$15x10^{-3}$- 35	[57]
Fluorescence	FRET, exonuclease catalyzed	$3x10^{-3}$	0.01 -100	[58]
Fluorescence	Ratiometric fluorescent aptasensor	$4,7x10^{-3}$	$2x10^{-3}$ -0,5	[59]
Fluorescence	Switchable fluorescence sensor	130	10-50	[23]
Fluorescence	Magnetic NP, rGO, DNase I	0.28	0.5- 30	[60]
Fluorescence	Ratiometric fluorescent aptasensor	$73x10^{-4}$	0,01–200	[61]
Colorimetric	Aptasensor, enzyme chromogenic	$48x10^{-3}$	$5x10^{-2}$ -2,5	[50]

analysis	colorimetric assay			
LC	UHPLC-MS/MS, aptamer functionalized monolithic capillary column, A1*	$3{,}34 \times 10^{-4}$	$12{,}32 \times 10^{-4}$- 1,232	[62]
QCM	MIP-sensor QCM	3.1	7.5 - 60	[63]
SERS	MIP-SERS, AuNPs	$8{,}3 \times 10^{-4}$	7.10^{-12}- $5.\ 10^{-8}$	[64]
Electrochemical	Au electrode, ZnO nanorods and chitosan, EIS and DPV, A1*	0.27×10^{-3}	5×10^{-4}–50	[65]
Electrochemical	GCE, black phosporus nanosheets, EIS, A1*	4.62×10^{-3}	154×10^{-4}– 540	[47]
Electrochemical	DNA walker, Pt@Au nanorods/ Fe-metal oxide films/ poly(ethylene imine) – rGO, CV *	4×10^{-5}	5×10^{-5} – 0.5	[66]
Electrochemical	Aptasensor, tetrahedral DNA nanostructure, thionine labelled Fe_3O_4 nanoparticles/ rGO	$3{,}04 \times 10^{-5}$	5×10^{-5}- 500	[67]
Electrochemical	Hierarchically porous Zn organic framework@ MB labeled aptamer, chitosan/ ZnO nanorods and AgNP, EIS and DPV detection	1.46×10^{-5}	5×10^{-5} - 0.5	[68]
Electrochemical	Carboxyl-amine modified polyethylene glycol spacer, diazonium salt reduction, carbon-SPE, EIS	2.8	1-25	[69]
Electrochemical	Structure switching aptasensor	3.56	1-25	**This Work**

References

[1] L. Xu, Z. Zhang, Q. Zhang, P. Li, *Toxins* **2016**, *8*, 239.

[2] N. Duan, S. Wu, S. Dai, H. Gu, L. Hao, H. Ye, Z. Wang, *Analyst* **2016**, *141*, 3942-3961.

[3] J. S. Câmara, P. Fernandes, N. Barros, R. Perestrelo, *Separations* **2023**, *10*, 149.

[4] Y. Bian, Y. Zhang, Y. Zhou, B. Wei, X. Feng, *Toxins* **2023**, *15*, 215.

[5] J. W. Bennett, M. Klich, *Clin Microbiol Rev* **2003**, *16*, 497-516.

[6] C. Gurikar, D. P. Shivaprasad, L. Sabillón, N. A. Nanje Gowda, K. Siliveru, *Grain & Oil Science and Technology* **2023**, *6*, 1-9.

[7] E. Janik, M. Niemcewicz, M. Ceremuga, M. Stela, J. Saluk-Bijak, A. Siadkowski, M. Bijak, *International Journal of Molecular Sciences* **2020**, *21*, 8187.

[8] L. Zhong, J. Carere, Z. Lu, F. Lu, T. Zhou, *Toxins* **2018**, *10*.

[9] G. L. Ngolong Ngea, Q. Yang, R. Castoria, X. Zhang, M. N. Routledge, H. Zhang, *Comprehensive Reviews in Food Science and Food Safety* **2020**, *19*, 2447-2472.

[10] G. Ianiri, A. Idnurm, S. A. I. Wright, R. Durán-Patrón, L. Mannina, R. Ferracane, A. Ritieni, R. Castoria, *Applied and Environmental Microbiology* **2013**, *79*, 3101-3115.

[11] M. M. Moake, O. I. Padilla-Zakour, R. W. Worobo, *Comprehensive Reviews in Food Science and Food Safety* **2005**, *4*, 8-21.

[12] J. Xu, J. Liu, W. Li, Y. Wei, Q. Sheng, Y. Shang, *Foods* **2023**, *12*.

[13] H. Pang, H. Li, W. Zhang, J. Mao, L. Zhang, Z. Zhang, Q. Zhang, D. Wang, J. Jiang, P. Li, *Toxins* **2022**, *14*, 272.

[14] G. Evtugyn, T. Hianik, *Chemosensors* **2019**, *7*, 10.

[15] A. Vidal, S. Ouhibi, R. Ghali, A. Hedhili, S. De Saeger, M. De Boevre, *food and chemical toxicology* **2019**, *129*, 249-256.

[16] N. Küçük, S. Şahin, M. O. Çağlayan, *Critical Reviews in Analytical Chemistry* **2023**, 1-13.

[17] G. Şahin, S. Ünüvar, T. Baydar, *Turk Pediatri Arsivi* **2011**, *46*, 275-279.

[18] X. Tang, Q. Zhang, M. Isabel Pividori, Z. Zhang, J.-L. Marty, G. Catanante, *Biosensors* **2022**, *12*, 59.

[19] A. Pennacchio, G. Ruggiero, M. Staiano, G. Piccialli, G. Oliviero, A. Lewkowicz, A. Synak, P. Bojarski, S. D'Auria, *Optical Materials* **2014**, *36*, 1670-1675.

[20] R. Paramastuti, W. P. Rahayu, S. Nurjanah, *Advances in Food Science, Sustainable Agriculture and Agroindustrial Engineering (AFSSAAE)* **2021**, *4*, 93-109.

[21] G. S. Shephard, N. L. Leggott, *Journal of Chromatography A* **2000**, *882*, 17-22.

[22] M. de Champdore, P. Bazzicalupo, L. De Napoli, D. Montesarchio, G. Di Fabio, I. Cocozza, A. Parracino, M. Rossi, S. D'Auria, *Analytical chemistry* **2007**, *79*, 751-757.

[23] R. Khan, T. A. Sherazi, G. Catanante, S. Rasheed, J. L. Marty, A. Hayat, *Food chemistry* **2020**, *312*, 126048.

[24] Q. Zhang, Y. Yang, C. Zhang, Y. Zheng, Y. Wu, X. Wang, *Food Control* **2021**, *119*, 107461.
[25] R. R. M. Paterson, Z. Kozakiewicz, T. Locke, D. Brayford, S. C. B. Jones, *Food Microbiology* **2003**, *20*, 359-364.
[26] E. Horváth, G. Papp, J. Belágyi, Z. Gazdag, C. Vágvölgyi, M. Pesti, *Food and Chemical Toxicology* **2010**, *48*, 1898-1904.
[27] D. Spadaro, A. Ciavorella, S. Frati, A. Garibaldi, M. L. Gullino, *Food Control* **2007**, *18*, 1098-1102.
[28] A. Ciegler, R. Vesonder, L. K. Jackson, *Applied and environmental microbiology* **1977**, *33*, 1004-1006.
[29] S. M. Nimjee, R. R. White, R. C. Becker, B. A. Sullenger, *Annu Rev Pharmacol Toxicol* **2017**, *57*, 61-79.
[30] X. Ni, M. Castanares, A. Mukherjee, S. E. Lupold, *Curr Med Chem* **2011**, *18*, 4206-4214.
[31] C. Tuerk, L. Gold, *Science* **1990**, *249*, 505-510.
[32] M. Çağlayan, *Current Analytical Chemistry* **2016**, *13*, 18-30.
[33] S. Şahin, Ş. Kaya, Z. Üstündağ, M. O. Caglayan, *Journal of Solid State Electrochemistry* **2022**, *26*, 907-915.
[34] S. Şahin, M. O. Caglayan, Z. Üstündağ, *Talanta* **2020**, *220*, 121437.
[35] C. Mustafa Oguzhan, *Current Analytical Chemistry* **2017**, *13*, 18-30.
[36] S. Şahin, M. Çağlayan, Z. Üstundağ, *Talanta* **2020**, *220*, 121437.
[37] X. Shkembi, M. Svobodova, V. Skouridou, A. S. Bashammakh, A. O. Alyoubi, C. K. O'Sullivan, *Analytical Biochemistry* **2022**, *644*, 114156.
[38] L. Ma, T. Guo, S. Pan, Y. Zhang, *Microchimica Acta* **2018**, *185*, 487.
[39] H. Pang, H. Li, W. Zhang, J. Mao, L. Zhang, Z. Zhang, Q. Zhang, D. Wang, J. Jiang, P. Li, *Toxins* **2022**, *14*.
[40] X. Yan, Y. Zhao, G. Du, Q. Guo, H. Chen, Q. He, Q. Zhao, H. Ye, J. Wang, Y. Yuan, T. Yue, *Chemical Engineering Journal* **2022**, *433*.
[41] Z. Guo, L. Gao, S. Jiang, H. R. El-Seedi, I. M. El-Garawani, X. Zou, *Journal of Food Composition and Analysis* **2023**, *115*.
[42] S. Liu, S. Meng, M. Wang, W. Li, N. Dong, D. Liu, Y. Li, T. You, *Food Chemistry* **2023**, *410*, 135450.
[43] N. Salandari-Jolge, A. A. Ensafi, B. Rezaei, *Analytical and Bioanalytical Chemistry* **2021**, *413*, 7451-7462.
[44] Y.-X. Chen, X. Wu, K.-J. Huang, *Sensors and Actuators B: Chemical* **2018**, *270*, 179-186.
[45] J. Xu, J. Liu, W. Li, Y. Wei, Q. Sheng, Y. Shang, *Foods* **2023**, *12*, 846.
[46] S. Liu, S. Meng, M. Wang, W. Li, N. Dong, D. Liu, Y. Li, T. You, *Food Chemistry* **2023**, *410*.
[47] J. Xu, X. Qiao, Y. Wang, Q. Sheng, T. Yue, J. Zheng, M. Zhou, *Microchimica Acta* **2019**, *186*, 238.

[48] L. R. Schoukroun-Barnes, F. C. Macazo, B. Gutierrez, J. Lottermoser, J. Liu, R. J. White, *Annu Rev Anal Chem (Palo Alto Calif)* **2016**, *9*, 163-181.

[49] L. R. Schoukroun-Barnes, F. C. Macazo, B. Gutierrez, J. Lottermoser, J. Liu, R. J. White, *Annual Review of Analytical Chemistry* **2016**, *9*, 163-181.

[50] S. Wu, N. Duan, W. Zhang, S. Zhao, Z. Wang, *Analytical Biochemistry* **2016**, *508*, 58-64.

[51] M. Zuker, *Nucleic Acids Research* **2003**, *31*, 3406-3415.

[52] C. Schmidt, A. Kammel, J. A. Tanner, A. B. Kinghorn, M. M. Khan, W. Lehmann, M. Menger, U. Schedler, P. Schierack, S. Rödiger, *Scientific Reports* **2022**, *12*, 2961.

[53] A. S. Lister, in *Separation Science and Technology, Vol. 6*, Elsevier, **2005**, pp. 191-217.

[54] Ş. F. Küçükayar, V. Şimşek, M. O. Caglayan, Z. Üstündağ, S. Şahin, *Microchemical Journal* **2023**, *193*, 109023.

[55] A. Zinedine, J. M. Soriano, J. C. Moltó, J. Mañes, *Food and Chemical Toxicology* **2007**, *45*, 1-18.

[56] R. Khan, T. A. Sherazi, G. Catanante, S. Rasheed, J. L. Marty, A. Hayat, *Food Chemistry* **2020**, *312*.

[57] A. Ahmadi, N. M. Danesh, M. Ramezani, M. Alibolandi, P. Lavaee, A. S. Emrani, K. Abnous, S. M. Taghdisi, *Talanta* **2019**, *204*, 641-646.

[58] Z. Wu, E. Xu, Z. Jin, J. Irudayaraj, *Food Chemistry* **2018**, *249*, 136-142.

[59] J. Deng, J. Hu, J. Zhao, Z. Zhang, Q. Wang, R. Wu, *Arabian Journal of Chemistry* **2022**, *15*, 103569.

[60] L. Ma, T. Guo, S. Pan, Y. Zhang, *Microchimica Acta* **2018**, *185*.

[61] J. Li, S. Li, Z. Li, Y. Zhou, P. Jin, F. Zhang, Q. Sun, T. Le, Jirimutu, *Talanta* **2023**, *257*, 124296.

[62] Q. Zhang, Y. Yang, C. Zhang, Y. Zheng, Y. Wu, X. Wang, *Food Control* **2021**, *119*.

[63] Y. Lin, G. Xu, F. Wei, A. Zhang, J. Yang, Q. Hu, *Journal of Pharmaceutical and Biomedical Analysis* **2016**, *121*, 135-140.

[64] L. Wu, H. Yan, G. Li, X. Xu, L. Zhu, X. Chen, J. Wang, *Food Analytical Methods* **2019**, *12*, 1648-1657.

[65] B. He, X. Dong, *Microchimica Acta* **2018**, *185*.

[66] B. He, X. Dong, *Chemical Engineering Journal* **2021**, *405*.

[67] B. He, X. Lu, *Analytica Chimica Acta* **2020**, *1138*, 123-131.

[68] B. He, X. Dong, *Sensors and Actuators, B: Chemical* **2019**, *294*, 192-198.

[69] R. Khan, S. B. Aissa, T. A. Sherazi, G. Catanante, A. Hayat, J. L. Marty, *Molecules* **2019**, *24*.